CHEMISTRY
A European Journal

A Journal of
ChemPubSoc Europe

Accepted Article

Title: Energy transfer contribution from singlet state to the sensitization of Eu3+ and Tb3+ luminescence by sulfonylamidophosphates and the role of the 7F5 level of Tb3+ in this process

Authors: Ewa Kasprzycka, Victor A. Trush, Vladimir M. Amirkhanov, Lucjan Jerzykiewicz, Oscar L. Malta, Janina Legendziewicz, and Paula Gawryszewska

This manuscript has been accepted after peer review and appears as an Accepted Article online prior to editing, proofing, and formal publication of the final Version of Record (VoR). This work is currently citable by using the Digital Object Identifier (DOI) given below. The VoR will be published online in Early View as soon as possible and may be different to this Accepted Article as a result of editing. Readers should obtain the VoR from the journal website shown below when it is published to ensure accuracy of information. The authors are responsible for the content of this Accepted Article.

To be cited as: *Chem. Eur. J.* 10.1002/chem.201603767

Link to VoR: http://dx.doi.org/10.1002/chem.201603767

Supported by
ACES

WILEY-VCH

10.1002/chem.201603767

WILEY-VCH

Energy transfer contribution from singlet state to the sensitization of Eu^{3+} and Tb^{3+} luminescence by sulfonylamidophosphates and the role of the $^7F_5$ level of Tb^{3+} in this process

Ewa Kasprzycka[a], Victor A. Trush[b], Vladimir M. Amirkhanov[b], Lucjan Jerzykiewicz[a], Oscar L. Malta[c], Janina Legendziewicz[a], Paula Gawryszewska*[a]

Abstract: A series of stable lanthanide complexes $Na[Ln(L)_4]$ (Ln = La^{3+}, Eu^{3+}, Gd^{3+}, Tb^{3+}, L = $[L^1]^-$, $[L^2]^-$), with dimethyl(4-methylphenylsulfonyl)amidophosphate (**HL^1**) and dimethyl 2-naphthylsulfonylamidophosphate (**HL^2**), here denoted as **1Ln**, **2Ln**, as well as sodium salts, **NaL**, denoted as **1Na**, **2Na** were synthesized. The compounds were characterized by single-crystal X-ray diffraction, IR, absorption and emission spectroscopies at 293 and 77 K. In contrast to the usual and well known dominant role of the ligand triplet state in intramolecular energy transfer processes in Ln complexes, in this particular new class of Ln compounds with sulphonylamidophosphate ligands we discuss, for the first time, the strong experimental and detailed theoretical evidences that suggest a dominant role played by the ligand first excited singlet state. The importance of the role played by the $^7F_5$ level in the case of the Tb^{3+} compound in this process is shown. The theoretical approach for the energy transfer rates was successfully applied to the rationalization of the experimental data. The higher lying excited levels of Eu (^5D_J, ^5L_J, ^5G_J) and Tb (^5D_J, ^5G_J, ^5L_J, ^5H_J, ^5F_J, ^5I_J) were included in the calculations for the first time. Both the multipolar and exchange mechanisms were taken into account. The experimental intensity parameters (Ω_λ), emission lifetimes (τ), radiative (A_{rad}) and non-radiative (A_{nrad}) decay rates, quantum yields (theoretical and experimental) were determined and discussed in detail.

Introduction

Lanthanide chelates are of great interest due to their special luminescence properties and their various applications for technological purposes [1-3]. Luminescence of these ions is characterized by: large Stokes shift upon excitation in the ligand states (in the UV) and subsequent 4f-4f emission in the near UV, visible or IR spectral regions, narrow emission bands and long luminescence decay times (millisecond scale) [1,2]. Because of the low value of the molar absorption coefficient, associated with intraconfigurational 4f-4f transitions, a strongly sensitized lanthanide photoluminescence is achieved by excitation of a chelating chromophore to its singlet state followed by efficient energy transfer from the absorber to the metal ion excited state (the so-called antenna effect) [1,2,4]. Due to the apparent Stokes shift and their quite different characteristics between excitation and emission, these types of compounds have been referred to as light converting molecular devices (LCMDs) [5].

LCMDs put out different requirements on the range of absorption and emission wavelength depending on their intended use. However, all LCMDs must exhibit an effective sensitized emission. To achieve this, three conditions must be fulfilled: (i) efficient absorption process, (ii) efficient energy transfer from the excited levels of the ligand to the emitting center and (iii) efficient luminescence. Many studies on the lanthanide chelates apply to one of these individual processes. However, the final 4f-4f luminescence quantum yield depends on a balance between them, including non-radiative decay channels, in the compound. Correlation between experimental and theoretical results gives the opportunity to test and to improve the functioning of theoretical models, and to understand the mechanisms of intramolecular energy transfer, which can be a tool for the design of new compounds with functional optical properties.

The commonly observed sensitization process for luminescent Eu^{3+} and Tb^{3+} complexes involves a triplet pathway, in which the transfer of the energy absorbed by the ligand to the Ln^{3+} ion takes place from the ligand-centered triplet excited state (T_1) [6-8]. Among thousands of publications on lanthanide complexes, only a few have included evidences of a dominant singlet (S_1) pathway [9-22]. Dominant singlet energy transfer has seldom been observed, in the sensitization of lanthanide ions, because intersystem crossing ($S_1 \rightarrow T_1$) is usually very fast due to not only the rather small $S_1 - T_1$ energy difference ($\cong$ 5000 cm^{-1}), but also to the external heavy atom effect induced by the lanthanide ion. Particularly a few papers relate to Eu^{3+} [12-16] and Tb^{3+} [23-26]. In the case of Tb^{3+} chelates, the singlet pathway may be of relevance particularly when the ligand triplet state lies below or very close to the emitting $^5D_4$ state, a situation in which luminescence quenching is normally observed. The theoretical challenge of describing intramolecular energy transfer processes that occur between a ligand and a lanthanide ion in luminescent complexes, including selection rules, was first treated in detail in references [5, 27, 28]. Expressions for transfer rates corresponding to the so-called direct Coulomb and exchange mechanisms have been obtained, from which selection rules could be derived [29].

[a] E. Kasprzycka, Dr. L. Jerzykiewicz, Prof. Dr. J. Legendziewicz, Dr. P. Gawryszewska
Faculty of Chemistry
University of Wroclaw
14 F. Joliot-Curie Str., 50-383 Wroclaw, Poland
E-mail: paula.gawryszewska@chem.uni.wroc.pl
[b] Dr. V. A. Trush, Prof. Dr. V. M. Amirkhanov
Department of Chemistry
Taras Shevchenko National University of Kyiv
Volodymyrska str. 64, Kyiv 01601, Ukraine
[c] Prof. Dr. O. L. Malta
Departamento de Química Fundamental
Universidade Federal de Pernambuco
Cidade Universitária, Recife-PE, 50740-560, Brazil

Supporting information for this article is given via a link at the end of the document.

Accepted Manuscript

This article is protected by copyright. All rights reserved.

The literature related to the studies on the photophysical properties of Ln complexes with the antenna effect is very broad. The most widely investigated group of complexes are the compounds with β-diketones [30-33], which are known as excellent emission sensitizers in complexes with lanthanide ions. With that in mind we undertook a study of a new class of lanthanide complexes, sulfonylamidophosphates, which are the S, N, P hetero analogues of *β*- diketones. The structure of the ligands has been planned in such a way as to decrease the multiphonon quenching of lanthanide emission in comparison to their complexes with *β*- diketones. This has been achieved by a replacement of C=O vibrations (~1600 cm^{-1}) by the lower energetic vibrations P=O (~1250 cm^{-1}) and S=O (~1350 cm^{-1}). Moreover, in the complexes with sulfonylamidophosphates in six-membered chelate ring created as a result of coordination with the lanthanide ion, the high-frequency C-H vibrations present in beta-diketonates do not occur. Additionally, the presence of the phosphorus atom in our ligands raises the possibility of bonding with the additional chromophore, in relation to the carbon atom, which enables stronger sensitization of the emission of the lanthanide ions. Furthermore, these complexes constitute a new partition of coordination chemistry of this type of ligands, creating simultaneously a new class of lanthanide complexes with ligands possessing the structural fragment -SO_2NHP(O)-. During the past few years, much effort has been devoted to the investigation of the coordination behavior and photophysical properties of these kinds of complexes with f-metals [34-38]. Continuing our study of lanthanide complexes with sulphonylamidophosphate ligands, the mechanisms of ligand-to-metal energy transfer in the new europium and terbium complexes with dimethyl(4-methylphenylsulfonyl)amidophosphate (**HL^1**) and dimethyl 2-naphthylsulfonylamidophosphate (**HL^2**) (Figure 1) were examined for the first time in this class of complexes. For the calculations of the energy transfer rates, an unprecedented number of Eu and Tb excited levels was included, and the important role played by the $^7F_5$ level of Tb^{3+} in the energy transfer process was discussed. The reasons for unexpected results that emerge, such as strong experimental and theoretical evidences that sulfonylamidophosphates-to-Ln^{3+} energy transfer occurs mainly from the singlet states of our ligands were also investigated.

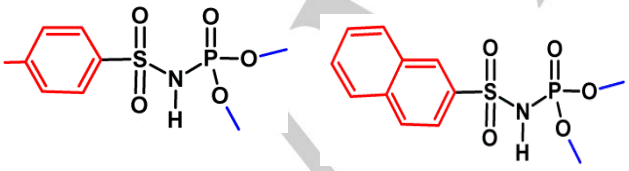

Figure 1. Structural formulae of the ligands.

Results and Discussion

X-ray Analysis

Single-crystal X-ray diffraction data show that the structures of **1Eu** and **2Eu** are monoclinic with the space group *C2c* and *C2*, respectively. The complexes of La^{3+}, Gd^{3+}, and Tb^{3+} are isostructural with the Eu^{3+} ones. The crystallographic data of **1Tb**, **1Eu** and **2Eu** is presented in Table S1. The molecular structures of **1Eu** and **2Eu** containing the numbering scheme for atoms are displayed in Figure 2 and 3, respectively.

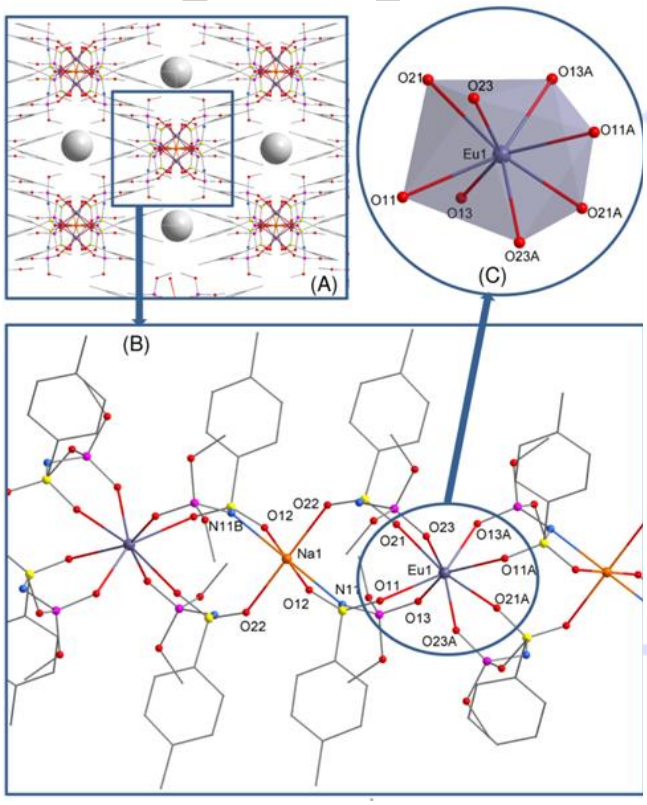

Figure 2. The X-ray structure of **1Eu**: view of crystal packing along the c-axis, molecular structure of **1Eu** (H atoms as well as dioxane molecules are omitted for clarity), coordination polyhedron of the Eu ion.

Accepted Manuscript

This article is protected by copyright. All rights reserved.

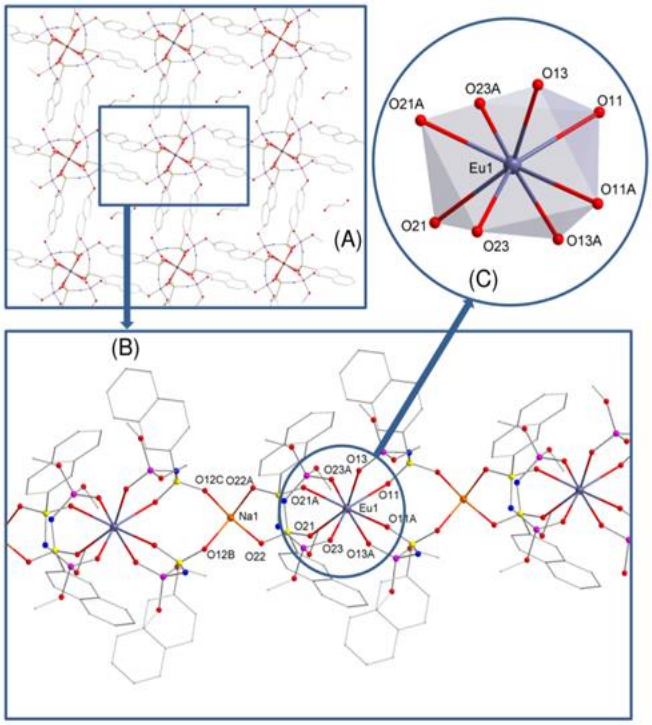

Figure 3. The X-ray structure of **2Eu**: view of crystal packing along the b-axis, molecular structure of **2Eu** (H atoms as well as dioxane molecules are omitted for clarity), coordination polyhedron of the Eu ion. Symmetry code: A 1-x, y, 1-z; B 1-x, 1-y, 1-z; C x, 1+y, 1-z.

In both complexes, the Eu^{3+} ions are eight-coordinated with the primary coordination sphere made up of four deprotonated ligands. One sulfonyl oxygen atom and one phosphoryl oxygen atom of each ligand are involved in europium-ion coordination. The six-membered chelating rings are formed, with the Ln-O bond lengths falling within the expected range (see Table S2). The Ln-O(S) distances are about 0.15 Å longer than the Ln-O(P) distances for **1Eu** and **2Eu**. The Tb–O distances are shorter than the corresponding Eu–O ones due to lanthanide contraction. The coordination polyhedron of the lanthanide ions can be described as a slightly distorted dodecahedron, based on a criterion proposed by Porai-Koshits and Aslanov [39]. The value of angles for ideal polyhedrons and for polyhedrons of **1Eu** and **2Eu** are shown in Tab. S3. The selected angles in **1Eu**, **1Tb** and **2Eu** are presented in Tables S4a,b.

The Na ions connect the $[Ln(L)_4]^-$ units in the complexes, resulting in the creation of the polymeric chains along the c (**1Ln**) and b (**2Ln**) axis. In **1Eu**, the coordination number of Na ions equals six, due to the bonding with two sulphonyl oxygen atoms and one nitrogen atom from one complex anion, and another two sulphonyl oxygen atoms and a nitrogen atom from the neighboring ones. In **2Eu**, the Na ion is tetra-coordinated by sulphonyl oxygen atoms of four ligands, adopting tetrahedral geometry. The coordination number equal to 4 is not typical for sodium ion and may result from crystal packing. Similar geometry of the Na surrounding is observed for $Na[Nd(C_{14}H_{21}N_3O_5PS)_4]$ [40], $Na[Tb(C_{20}H_{19}NO_5PS)_4]$ [41].

Intra- and intermolecular non-covalent interactions play a role in the crystal packing and stabilize the structure. A weak intramolecular CH-π interaction (-OCH_3 with naphthyl ring) within each ligand exists for **2Eu**. The CH hydrogen atoms tend to point toward the center of the aromatic ring. The distances C11H11C…Cp1 (Cp1: C13, C14, C15, C20, C21, C22) centroid and C31H31B…Cp3 [1-x, y, 1-z] (Cp3: C33, C34, C35, C40, C41, C42) equal 2.86 and 2.85 Å, respectively. Such interactions are not found between the molecules in the chain or the inter-chains. A number of short CH-*π* distances has been previously shown in the crystal structures of organic compounds and it was suggested that the CH-*π* interaction constitutes one of the important factors in controlling the crystal packing of the molecules [42]. Molecules of dioxane in the outer coordination sphere of **2Eu** were observed. These solvent molecules are placed inside channels generated along the axis b. In turn, the relative position of the planes of naphthyl rings eliminates the existence of intermolecular π-π interactions in the chain and between chains. The π-π interactions do not occur in the **1Eu** complex while there are weak CH-*π* interactions (C12H12A…Cg(C13C14C15C16C17C18) – 2.98 Å and C22H22C…Cg(C23C24C25C26C27C28) – 3.00 Å). Disordered molecules of acetonitrile were observed in the outer coordination sphere of **1Eu**.

The measured Ln-Ln distances in both complexes were large, equal to 11.232 (**1Eu**) and 11.268 Å (**2Eu**) within the chains and 12.058 (**1Eu**) and 13.424 Å (**2Eu**) between the chains. Eu^{3+} is at the two-fold axis and Na^+ is on the inversion center in **1Eu**. In **2Eu** the Eu^{3+} and Na^+ ions are located on the twofold axis.

Spectroscopic Results

IR spectroscopy

The IR spectra of the Eu compounds and HL ligands were recorded in the range of 50-4000 cm^{-1} (see Fig. S1). IR spectroscopy for sodium salts (**1Na**, **2Na**) and complexes (**1Eu**, **2Eu**) shows the disappearance of the corresponding N-H vibration band of the free ligand. This is due to the fact that the ligands are deprotonated in the coordination compounds. The vibration of the amide group of $\mathbf{HL^2}$ appears in the region of 2450-2825 cm^{-1}, while for $\mathbf{HL^1}$ it is located between 2430 and 2847 cm^{-1}. Their maxima are at 2734 cm^{-1} and 2720 cm^{-1}, respectively. In the spectra of the free ligands $\mathbf{HL^1}$ and $\mathbf{HL^2}$, two characteristic sharp bands are observed with the maxima at 1234, 1341 cm^{-1} and 1246, 1338 cm^{-1}. They are assigned to the ν(P=O) and ν(S=O) vibrations. These bands appear for the **1Eu** and **2Eu** complexes at lower wavenumbers because of the coordination to the metal ion. The differences in frequencies for these groups are 77 cm^{-1} ($\Delta_{P=O}$), and 102 cm^{-1} ($\Delta_{S=O}$) for **1Eu** and 61 cm^{-1} ($\Delta_{P=O}$), and 89 cm^{-1} ($\Delta_{S=O}$) for **2Eu**. The O-Ln-O fragment related to the chelate ring, formed by the coordination is localized in the far infrared region. It is observed in the region 55-290 cm^{-1} as broad and middle intensity bands.

Electronic states of the ligands

Accepted Manuscript

This article is protected by copyright. All rights reserved.

The room temperature absorption spectra of transparent KBr tablets with **1Tb** and **2Tb** in the UV region are presented in Figure 4. The absorption spectra in this region consist of three bands in the ranges >212, 212-255, 255-325 and 200-255, 255-305, 305-340 nm for **1Tb** and **2Tb**, respectively. These bands are associated with $\pi \rightarrow \pi^*$ transitions characteristic for phenyl and naphthyl chromophores, for some of which vibronic structure is seen. The barycenter of excited singlet states in the complexes and their half-width determined on the basis of Gaussian distributions of these absorption spectra amounts to 35088 cm^{-1}/6400 cm^{-1} and 31278 cm^{-1}/2000 cm^{-1} for **1Ln** and **2Ln**, respectively. Fitting of the spectra, the results of which are presented in Fig. S2, was performed with Gaussian function curves, yielding R^2 equal to 0.999 (**1Tb**) and 0.998 (**2Tb**). Having compared the intensity ratios and shapes of the bands in the range of 255-325 nm between **1La** and **1Tb** as well as in the range of 260-340 between **2La** and **2Tb,** it was difficult to exclude with certainty the presence of f-d transitions in Tb complexes in mentioned energy ranges. Furthermore, no additional band or widening of the absorption spectra of **1Eu** and **2Eu** complexes, as compared to **1La** and **2La**, could be seen. In these cases, ligand-to-metal charge transfer states (LMCT) could be covered by the bands of the ligands. According to the theoretical calculations reported by Faustino and co-authors the energy transfer rate $S_1 \rightarrow$ LMCT for the same energy positions of S_1 and LMCT is about 10^9 s^{-1} [43]. The LMCT state takes usually part in quenching of sensitized luminescence. The relaxation to the ground state via the crossover process to C-T states in Eu complexes is very often strongly temperature dependent since these processes are usually phonon-assisted.

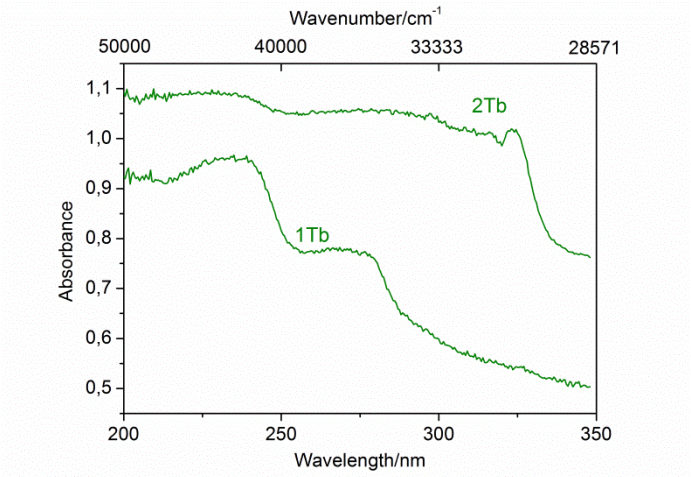

Figure 4. The absorption spectra of **1Tb** and **2Tb** as KBr pellets at 293 K.

Figure 5 presents the luminescence spectra of **1La** and **2La** in the solid state at 293 and 77 K and their excitation spectra. For both types of complexes, the fluorescence ($S_1 \rightarrow S_0$) at room temperature, with maxima at 295.5 nm (**1La**), 342 nm (**2La**), and the fluorescence and weak phosphorescence ($T_1 \rightarrow S_0$) at 77 K were measured. It is worth noting that for **2Na** and **2La** the phosphorescence observed in the range of 500 – 600 nm was too weak for the measurement of lifetime to be possible using our equipment. The phosphorescence of **2La** is not observable at an excitation wavelength of 290 nm, but can be observed for λ_{exc} = 330 nm (see Fig. 5).The Na and La compounds reveal a very similar intensity of the fluorescence, which is seen in Fig.6. Moreover, fluorescence lifetimes of **1La** and **2La** are almost the same as for **1Na** and **2Na**, respectively (see Tab. 1b).

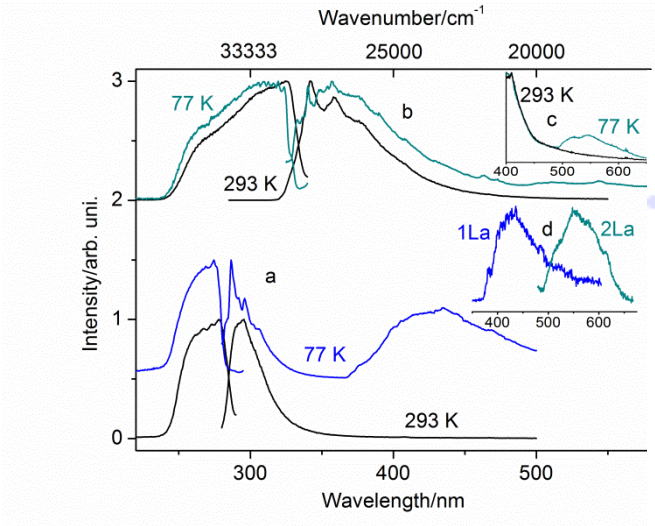

Figure 5. The luminescence and excitation spectra of a) **1La** (λ_{exc}=270 nm, λ_{mon}=300nm); b) **2La** ((λ_{exc}=290 nm, λ_{mon}=345nm) in solid state at 293 and 77K; c) the luminescence spectra of **2La** at 293 and 77 K (λ_{exc}=330 nm). The inset shows phosphorescence spectra of **1La** after switching off the excitation source (the fourth harmonic (266 nm) of an Nd:YAG pulsed laser) and **2La** (λ_{exc}=330 nm, xenon lamp).

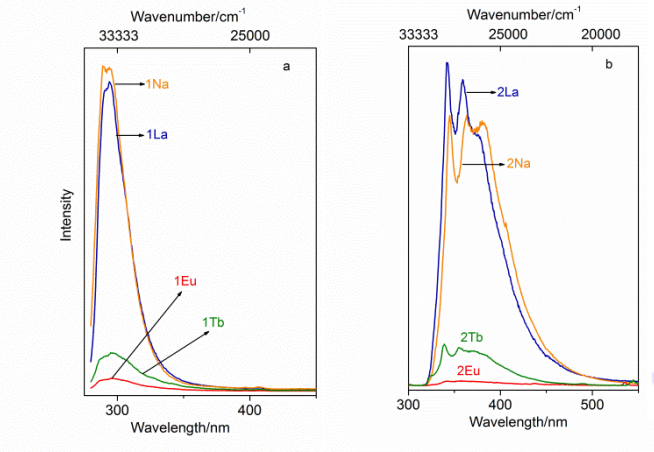

Figure 6. The dependence of the fluorescence intensity for a) **1Na**, **1La**, **1Eu**, **1Tb** (λ_{exc}=270 nm), b) **2Na**, **2La**, **2Eu**, **2Tb** (λ_{exc}=290 nm) at 293 K.

Accepted Manuscript

This article is protected by copyright. All rights reserved.

Table 1. a) Decay time of $^5D_0$, $^5D_1$ and $^5D_4$ emission for **1Eu** (λ_{exc} = 300 nm), **1Tb** (λ_{exc} = 280 nm), **2Eu**, **2Tb** (λ_{exc} = 320 nm) at 293 and 77K.

	1Eu ($^5D_0$)	**1Eu** ($^5D_1$)	**1Tb** ($^5D_4$)	**2Eu** ($^5D_0$)	**2Eu** ($^5D_1$)	**2Tb** ($^5D_4$)
τ 293 K /ms	2.51 0.013 rise time	0.0135	2.78	1.47 2.10 0.0094 rise time	0.0096	0.0108 0.0274
τ 77 K /ms	2.51		2.79	1.73 2.22		1.08 2.27

For excitation at 464 nm, the decay time of $^5D_0$ of **2Eu** equals 1.77 ms.

The decay time values were estimated with an error of 3%

Table 1. b) Decay time of fluorescence for **1Na**, **1La** (λ_{exc} = 280nm, λ_{mon} = 295 nm) and **2Na**, **2La** (λ_{exc} = 314 nm, λ_{mon} = 342 nm) at 293 K

	1Na	**1La**	**1Eu**	**1Tb**	**2Na**	**2La**	**2Eu**	**2Tb**
τ /ns	12.5	12		2.35	10	15	7.4	4.4

In the majority of lanthanide complexes, the ligands relax non-radiatively to their triplet states and spin forbidden $^1\pi\pi^* \rightarrow {}^3\pi\pi^*$ intersystem crossing (ISC) is induced by spin-orbit coupling enhanced through the presence of a heavy lanthanide. The presence of fluorescence in **1La**, **2La** at 293 and 77 K and the same values of fluorescence lifetime for La and Na compounds indicate that the $S_1 \rightarrow S_0$ process of depopulation of the ligand singlet state competes with the ISC, and that the investigated complexes have low intrinsic ISC, i.e. the heavy-atom effect is unnoticeable. The highly possible reason for this is the large energy gap between the singlet state and the triplet state, which is 11800 and 13300 cm^{-1} for the **1Ln** and **2Ln** complexes respectively, and the low heavy atom effect due to the large distance (5.8Å) between the donor chromophore and the Ln ion. It was shown in ref [44] that ISC is maximized when the energy difference between $^1\pi\pi^*$ and $^3\pi\pi^*$ amounts to ca. 5000 cm^{-1}. In turn, in ref. [10] the authors, apparently not observing the external heavy-atom effect, reported that the presence of a tertiary amine, which has an abnormal quadrupole moment, could be responsible for the highly forbidden character of the $S_1 \rightarrow T_1$ transition.

On the basis of the weak phosphorescence which accompanied fluorescence (the inset in Fig.5), the barycenter of the triplet states of the **1Ln** (E_{1T1}) and **2Ln** (E_{1T2}) complexes were determined as 23260 and 18000 cm^{-1}. Decay curves of the **1Gd** phosphorescence are reproduced by two exponentials (τ_1 = 1.1 ms and τ_2 = 4.7 ms, R^2 = 0.9997). Furthermore, the phosphorescence decay contains a weak long lasting component of the order of 20 ms, contributing a few percent to the total decay time.

Photoluminescence of lanthanide complexes

Figs.7 and S3 present the high resolution emission spectra at 293 and 77 K of the **1Eu**, **2Eu** and **1Tb**, **2Tb** crystals respectively. The bands correspond to the well-known $^5D_0 \rightarrow {}^7F_J$ (J = 0-4) and $^5D_4 \rightarrow {}^7F_J$ (J = 0-6) transitions. For **2Tb**, we see very weak emission at 293 K because the ligand triplet state is below the Tb^{3+} emitting state ($^5D_4$) and the energy difference between T_{1L2} (barycenter) and $^5D_4$ is 2614 cm^{-1}. The $^5D_0 \rightarrow {}^7F_2$ and $^5D_4 \rightarrow {}^7F_5$ transitions dominate the Eu and Tb spectra respectively, which indicate that the lanthanide ions occupy sites without an inversion center. The emission spectra of **1Eu** and **2Eu** as well as **1Tb** and **2Tb**, for each pair of ions, are very similar in the profile, splitting and energy of the transitions. The reason for this is the strong resemblance of inner coordination sphere and coordination polyhedron (described as a slightly distorted dodecahedron) of lanthanide ions in **1Ln** and **2Ln** (see paragraph 2.1).

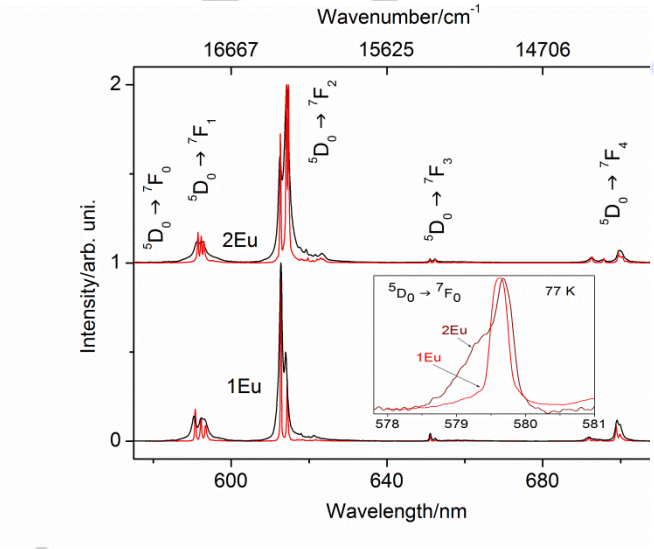

Figure 7. The emission spectra of **1Eu** (λ_{exc}=300 nm) and **2Eu** (λ_{exc}=320 nm) at 293 (black line) and 77 K (red line).

The emission spectra at 77 K of **1Eu** revealed a single component of $^5D_0 \rightarrow {}^7F_0$ transition at 579 nm (17253 cm^{-1}) with a width at half-height equal to 9 cm^{-1}, which is consistent with only one site being occupied by the Eu^{3+} ions. On the other hand, the $^5D_0 \rightarrow {}^7F_0$ band of the 2Eu site is two-fold (see inset in Fig.7). The two components of this band were derived from a Gaussian curve fitting procedure with the maxima at 579 nm (17260 cm^{-1}) and 579.7 nm (17250 cm^{-1}). This probably results from the disorder of the Eu^{3+} ions, which are on a two-fold axis of symmetry, because after the final refinement cycle for **2Eu** single crystal, large residual electron density peaks (2.0 and 1.6 e/Å^3) remain near the Eu ion. This possibly is an unrecognized twinning associated with the crystal data and a disordered with respect to the Eu sublattice, which provides most of the resonant contribution. However, the emission spectrum of **2Eu** (similarly to **1Eu**) at 77 K shows three well separated electronic lines due to the magnetic dipole $^5D_0 \rightarrow {}^7F_1$ transition, suggesting the presence of a single major chemical environment around the Eu^{3+} ion [45]. The analysis of the Stark components for the $^5D_0 \rightarrow {}^7F_J$ transitions at 77 K suggests that the Eu^{3+} symmetry sites in **1Eu** and **2Eu** are close to D_2 [46]. This is in line with the

Accepted Manuscript

This article is protected by copyright. All rights reserved.

discussion about the coordination polyhedra in the **1Ln** and **2Ln** complexes.

It should be noted that for both Eu complexes the $^5D_1$ emission is observed at room and low temperature, which is presented in Fig. S4. In this case, the competition of two processes is responsible for the emission from the $^5D_1$ state: multiphonon relaxation, which feeds the $^5D_0$ state, and $^5D_1 \rightarrow {}^5D_0, {}^7F_0 \rightarrow {}^7F_3$ cross-relaxation process. In both investigated compounds the Eu-Eu distances are large (of the order 11 Å), suggesting the inefficient $^5D_1 \rightarrow {}^5D_0, {}^7F_0 \rightarrow {}^7F_3$ cross-relaxation. As is known from the literature, the $^5D_1$ emission from europium complexes with organic ligand is observed even when high energy oscillations are present in the inner coordination sphere (e. g. ≈ 1300 cm^{-1}, ≈1600 cm^{-1}, ≈ 2900 cm^{-1} or ≈3600 cm^{-1}) [47-50].

The values of emission lifetimes of the $^5D_0$, $^5D_1$ and $^5D_4$ levels are presented in Tab. 1. The decay profiles of emission are monoexponential for **1Eu** (Fig. S5), **1Tb** (Fig. S6), mono- or biexponential for **2Eu** (Fig. S7) and biexponential for **2Tb** (Figs. S8a, b). For the fit of the experimental data, coefficient of determination R^2 equal to 0.999 was obtained. The spectra of $^5D_0$ emissions were also fitted using a function containing exponential rising and decaying parts. Lifetime values of the **1Eu** ($^5D_0$) and **1Tb** ($^5D_4$) emissions are temperature and excitation wavelength independent, and thus reflect the absence of thermally activated non-radiative processes, either vibrational or electronic in nature, including the emitting levels $^5D_0$ and $^5D_4$. A discussion of emission lifetimes of the $^5D_0$ and $^5D_4$ levels for **2Eu** and **2Tb** is included in the **section Analysis of energy transfer.**

In Table 1, rise times of the emitting $^5D_0$ levels of **1Eu** and **2Eu** are included. These luminescence rise times perfectly match the decay times of $^5D_1$ emission, which indicates that the $^5D_0$ is populated directly from the $^5D_1$ level. Decay times of $^5D_1$ emission and rise time of $^5D_0$ emission equal to 13 and 13.5 μs (**1Eu**) and 9.6 and 9.4 μs (**2Eu**) respectively, were measured at 293 K. The correlation between the temperature dependent rise time of the $^5D_0$ emitting level and decay time of the $^5D_1$ excited level in a europium complex has been discussed by Faustino et al [51].

Analysis of energy transfer

The efficiency of ligand-to-metal energy transfer is reflected in the excitation spectra. The excitation spectra at 293 and 77 K for the **1Eu** and **1Tb** complexes are plotted in Fig. 8. They consist of a broad band in the range 240 – 325 nm, arising from the absorption transition to the ligand singlet state, and narrow lines of the f-f transitions of the Eu^{3+} and Tb^{3+} ions. The broad band dominates the excitation spectra of **1Tb**, which proves a relatively efficient ligand to metal energy transfer. In the spectra of **1Eu**, f-f transitions dominate, indicating less efficient ligand–to-metal energy transfer. Efficiency of energy transfer in **1Eu** and **1Tb** are nearly temperature independent, as evidenced by the constant value of the intensity ratio of $^7F_0 \rightarrow {}^{2S+1}L_J$/ $\pi \rightarrow \pi^*$ transitions at 293 and 77K. However, the analysis of both excitation spectra combined together shows differences in the spectral range of 240-275 nm, where the **1Eu** excitation band has much lower intensity than in the range of 280-325, while the excitation band of **1Tb** is intense throughout the 240-325 nm range. This phenomenon indicate differences between **1Eu** and **1Tb** intramolecular energy transfer mechanisms. The participation of the 5d state in sensitiziation (range 240 – 275 nm) of the **1Tb** luminescence cannot be ruled out. Furthermore, we cannot completely exclude the participation of the LMCT state from the quenching of the sensitized luminescence of **1Eu.**

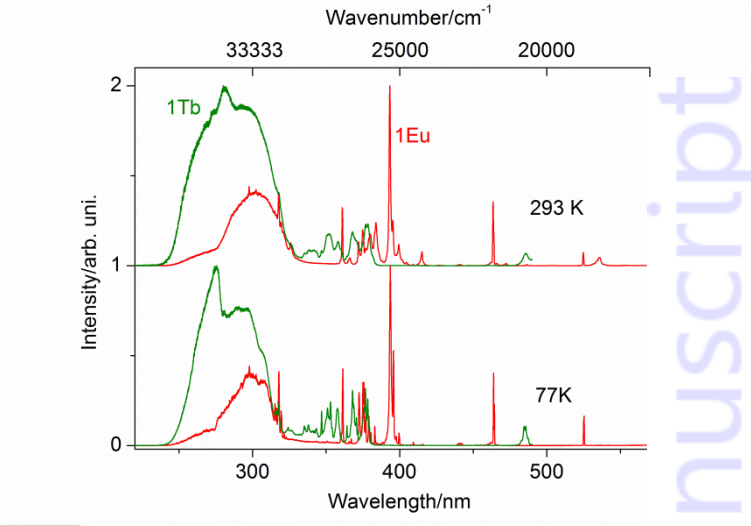

Figure 8. The excitation spectra of **1Eu** (red line, λ_{mon}=612.75 nm) and **1Tb** (green line, λ_{em}=546.5 nm) at 293 and 77 K.

The energy transfer rates W_{ETS} (energy transfer rates from $S_1 \rightarrow$ff* levels) and W_{ETT} ($T_1 \rightarrow$ff* levels) were calculated using a theoretical model described in literature [5, 25, 26] (see paragraph Theoretical Calculations**).** Table 2 presents the selected energy transfer rates for **1Eu** and **1Tb**. In Tables S5-S8 $U^{(\lambda)}$ squared reduced matrix element values, as well as values of M, and values of ff* energy transitions, and the energy difference between the ligand state and the lanthanide are listed. The energy transfer rate value correspond to the transitions between levels shown in Fig. 9. The Cartesian coordinates are gathered in Tab. S9 and corresponding to Figs. S9, S10, where the Ln ion is in the center of the coordinate system.

Accepted Manuscript

This article is protected by copyright. All rights reserved.

Table 2. Calculated values of total energy transfer rate from singlet (W_{ETS1}) and triplet (W_{ETT1}) states, total back energy transfer rate from singlet (W_{BETS1}) and triplet (W_{BETT1}) states, selected energy transfer rates and % contribution of each in overall energy transfer for **1Eu**, **1Tb**, **2Eu**, **2Tb**, the energy difference between barycenter of ligands states and lanthanide states (Δ).

1Eu	Δ /cm^{-1}	W /s^{-1}	Mechanism	%
W_{ETS1}	-	1.28x10^6	-	
$S_1 \rightarrow {}^5L_6$	975	3.81x10^5	Multipole	30
$S_1 \rightarrow {}^5G_3$	8834	2.21x10^5	Multipole	17
$S_1 \rightarrow {}^5D_3$	11045	2.09x10^5	Multipole	16
$S_1 \rightarrow {}^5G_6$	8235	1.61x10^5	Multipole	13
W_{ETT1}	-	4.06x10^2	-	0.03
$T_1 \rightarrow {}^5D_1$	4216	2.47x10^2	Exchange	0.02
1Tb	Δ /cm^{-1}	W/s^{-1}	Mechanism	%
W_{ETS1}	-	7.53x10^6	-	
$S_1 \rightarrow {}^5G_6$	8420	2.93x10^6	Both	39
$S_1 \rightarrow {}^5G_5$	7132	1.36 x10^6	Both	18
$S_1 \rightarrow {}^5L_7$	5556	1.15x10^6	Both	15
W_{ETT1}	-	2.11x10^3	-	0.03
$T_1 \rightarrow {}^5D_4$	2642	7.98 x10^2	Both	0.01
${}^5G_6 \rightarrow T_1$	3412	7.20 x10^2	Both	0.01
2Eu	Δ /cm^{-1}	W /s^{-1}	Mechanism	%
W_{ETS1}	-	1.80 x10^5	-	
$S_1 \rightarrow {}^5G_6$	4425	6.58x10^4	Multipole	36
$S_1 \rightarrow {}^5D_4$	3546	5.07x10^4	Multipole	28
$S_1 \rightarrow {}^5G_3$	5043	3.75x10^4	Multipole	21
W_{ETT1}	-	1003.5	-	0.60
${}^5D_1 \rightarrow T_1$	1040	577.77	Exchange	0.3
$T_1 \rightarrow {}^5D_0$	747.6	376.02	Multipole	0.2
2Tb	Δ /cm^{-1}	W /s^{-1}	Mechanism	%
W_{ETS1}	-	3.60x10^6	-	
$S_1 \rightarrow {}^5G_5$	3322	1.51x10^6	Both	42
$S_1 \rightarrow {}^5L_7$	1746	4.66x10^5	Exchange	13
$S_1 \rightarrow {}^5L_9$	2746	4.23x10^5		12
$S_1 \rightarrow {}^5L_8$	2030	4.07 x10^5		11
W_{ETT1}	-	2.34 x10^3	-	0.07
${}^5D_4 \rightarrow T_1$	2614	2.20x10^3	Exchange	0.06
W_{BETS1}	-	8.84x10^2	-	77
${}^5L_7 \rightarrow S_1$	1746	7.69x10^2	Exchange	67
W_{BETT1}	-	2.59 x10^2	-	23
$T_1 \rightarrow {}^5D_4$	2614	2.59 x10^2	Multipole	23

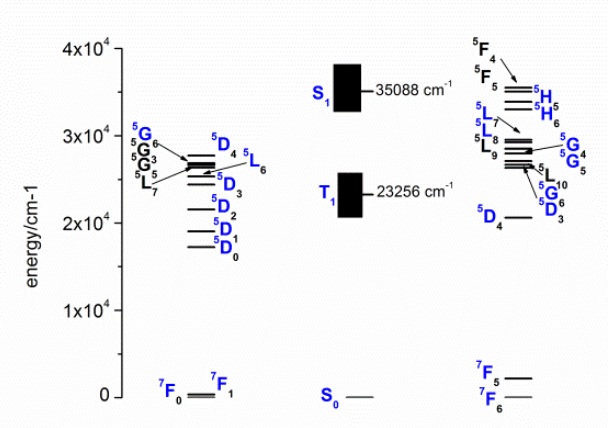

Figure 9. The energy level diagram for **1Eu** and **1Tb** used in the analysis of channels of emission sensitization.

In the case of both **1Eu** and **1Tb**, back-transfer rates were insignificant due to a negative energy mismatch Δ (>2000 cm^{-1}), which led to a small Boltzmann factor $e^{\frac{-\Delta}{k_B T}}$. In our analysis, we have considered energy transfer channels from ligand singlet state and ligand triplet state. The high lying excited levels of Eu (^5D_J, ^5L_J, ^5G_J) and Tb (^5D_J, ^5G_J, ^5L_J, ^5H_J, ^5F_J, ^5I_J) were included in the calculations for the first time. The direct transfer rates from S_1 to the $^5D_3$, $^5L_6$, $^5L_7$, $^5G_2$, $^5G_3$, $^5G_5$, $^5G_6$ levels for **1Eu** were calculated assuming a factor of thermal population equal to 0.33, at 293 K, for the $^7F_1$ manifold and an energy difference Δ=E(triplet) -[E($^5D_0$)-E($^7F_1$)]. According to the selection rules of energy transfer, direct energy transfer to the $^5D_0$ level is not allowed. This rule is, however, relaxed due to *J*-mixing effects and thermal population of the $^7F_1$ level [27, 28]. Taking into account the selection rules and the $^7F_{0,1}$ thermal populations at 293 K, the intramolecular energy transfer from S_1 to $^5D_3$, $^5L_7$, ^5L_J, $^5G_3$, $^5G_5$ levels becomes allowed through the multipolar (dipole-2$^\lambda$ pole and dipole-dipole) mechanisms ($|J\text{-}J'| \leq \lambda \leq |J\text{+}J'|$, $J' = J = 0$ are excluded) and the energy transfer to the $^5D_0$, $^5D_2$, $^5G_2$ becomes allowed through the exchange mechanism ($|J - J'| = 0\ or\ 1$, $J' = J = 0$ are excluded in the case of ligand-to-metal energy transfer) in **1Eu**. The main channels of energy transfer in **1Eu** and their percent contribution to the overall energy transfer from S_1 are: $S_1 \rightarrow {}^5G_6$ (13%), $S_1 \rightarrow {}^5G_3$ (17%), $S_1 \rightarrow {}^5D_3$ (16%), $S_1 \rightarrow {}^5L_6$ (30%) (see Tab. 2). As can be seen from the calculations (Tables 2 and S5, S6), the sum of energy rates for energy transfer from S_{1L1} and T_{1L1} in **1Eu** (W_{ETS1}=1.28x10^6 s^{-1}, W_{ETT1}=4.06x10^2 s^{-1}) is lower compared to that of **1Tb** (W_{ETS1}=7.53x10^6 s^{-1}, W_{ETT1}=2.11x10^3 s^{-1}). This is due to better resonance conditions between the ligand states (S_1, T_1) and the

Accepted Manuscript

This article is protected by copyright. All rights reserved.

excited levels of Tb^{3+} in comparison to the excited level of Eu^{3+}, as shown in the energy diagram in Fig. 9. The main channels of energy transfer in **1Tb** and their percent contribution to the overall energy transfer from S_1 are $S_1 \rightarrow {}^5G_6$ (39%), $S_1 \rightarrow {}^5G_5$ (18%) and $S_1 \rightarrow {}^5L_7$ (15%). The $T_1 \rightarrow {}^5D_4$ pathway plays a negligible role in **1Tb** (797 s^{-1}). Due to a large distance between donor and aceptor, taking as the distance between the lanthanide ion and the center of the phenyl ring (5.8 Å), the energy transfer rates are small for Eu^{3+} and Tb^{3+} levels for which the exchange mechanism dominates (Tab. S5, S6).

Similar situation was observed for **2Eu** and **2Tb** (Tab. S7, S8), where the Dexter energy transfer was disfavored by the lack of orbital contact between the donor and the acceptor. The main difference between the **1Ln** and **2Ln** complexes is a different energy match between ligand and Ln^{3+}, which we can observe at the energy diagram (Figs. 9, 10). Moreover, the barycenter of T_{1L2} is 2614 cm^{-1} below ${}^5D_4$ (20614 cm^{-1}) level of **2Tb**. Calculated values of the energy transfer rates also point at the dominating singlet energy transfer in **2Eu** and **2Tb**, where the sum of energy rates for energy transfer from S_{1L2} and T_{1L2} equal W_{ETS1}=1.80x10^5 s^{-1} (**2Eu**), W_{ETT1}=1.00x10^3 s^{-1} (**2Eu**) and W_{ETS1}=3,60x10^6 s^{-1} (**2Tb**), W_{ETT1}=2.34x10^3 s^{-1} (**2Tb**) (Tab. 2).

Basing on measurements of lifetimes and the calculations of non-radiative energy transfer rates, the main path of energy transfer is proposed for **2Eu** as $S_1 \rightarrow$ff* (mainly ${}^5G_6$, ${}^5D_4$ and ${}^5G_3$) $\rightarrow {}^5D_0$ and with a smaller contribution of $S_1 \rightarrow T_1 \rightarrow {}^5D_1 \rightarrow {}^5D_0$.

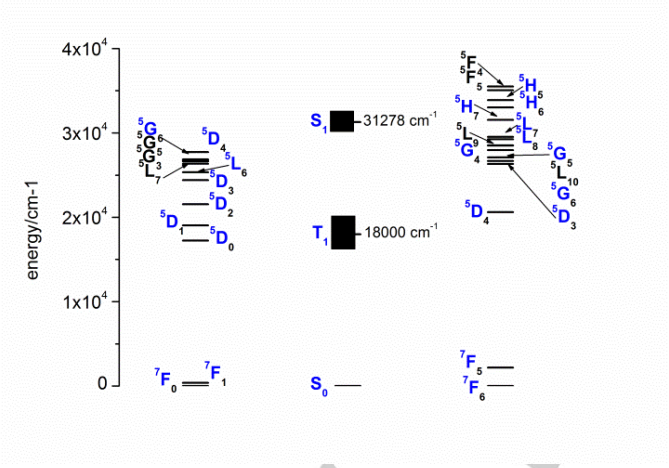

Figure 10. The energy level diagram for **2Eu** and **2Tb** used in the analysis of channels of emission sensitization.

The energy transfer process $T_{1L2} \rightarrow {}^5D_0$ in **2Eu**, mediated by the exchange mechanism, is slow (396 s^{-1}, 2.53 ms) but its participation in the energy transfer process is confirmed by the analysis of a dependence of the ${}^5D_0$ lifetime on the excitation wavelength (see Tab. 3). If ff* Eu^{3+} levels are excited directly using 394, 464 or 535.5 nm wavelength, the decays profiles of ${}^5D_0$ emission are monoexponential (1.7 ms), which is proved by respective residual plots. If the Eu^{3+} ion is excited indirectly into S_1 state of L^2 ligand, the decay profiles of the emission are biexponential (see Fig. S7). One component of the emission decay is almost the same (2.43 and 2.10 ms) as the $T_{1L2} \rightarrow {}^5D_0$ non-radiative energy transfer rate (2.53 ms), which suggests that ${}^5D_0$ level is populated through T_1 and obviously through the ${}^5D_1$ level. The contribution of this component in overall decay process diminishes with decreasing temperature from 293 K to 77 K from about 50% to about 20%. The absence of this component when the ff* levels are excited directly indicates that the T_1 state is populated as a results of intersystem crossing and not through the ${}^5D_1 \rightarrow T_{1L2}$ (578 s^{-1}, 1.73 ms) transition, which is too slow as compared to the ${}^5D_1 \rightarrow {}^5D_0$ transition (9 μs). The rise time of the emitting ${}^5D_0$ level has the same values either using direct or indirect excitation.

Table 3. The values of the emission decay times of the ${}^5D_0$ level for the excitation wavelength for **2Eu** at 293 and 77 K and the goodness of fit (χ^2).

Excitation wavelength /nm	Decay time 293 K /ms	χ^2	Decay time 77 K /ms	χ^2
291	1.63 2.43	1.015	1.76 2.34	1.130
322	1.47 2.10	1.005	1.73 2.22	1.159
394	1.77	1.199	1.75	1.123
464	1.78	1.026	1.76	1.002
535.5	1.78	1.030	1.77	1.003

In contrast to the **1Eu**, the temperature dependent sensitized emission is observed (Fig. 11) for **2Eu**. A presence of back energy transfer processes from ${}^5D_0$ into T_1 (ΔE = 750 cm^{-1}) was expected, but the values of lifetime at 293 and 77 K is almost the same and the value of the back energy transfer (${}^5D_0 \rightarrow T_1$) rate is low (W_{BET2} = 2.3 s^{-1}). As such, the contribution of the LMCT state with energy a little higher than for S_1 cannot be excluded. Especially, that the participation of LMCT in the quenching of the sensitized luminescence is a process which is usually temperature-dependent. The back energy transfer involving the S_1 state and ff* levels can be neglected (Tab. S7).

In the case of **2Tb**, the back energy transfer ${}^5L_7 \rightarrow S_{1L2}$ and $T_{1L2} \rightarrow {}^5D_4$ are present. The dominating singlet energy transfer $S_1 \rightarrow {}^5G_5$ (42%), $S_1 \rightarrow {}^5L_7$ (13%), $S1 \rightarrow {}^5L_9$ (12%) and $S_1 \rightarrow {}^5L_8$ (11%) (Tables 2 and S8) as well as competing processes ${}^5D_4 \rightarrow T_{1L2}$, $T_{1L2} \rightarrow {}^5D_4$, ${}^5D_4 \rightarrow {}^7F_J$ and $T_{1L2} \rightarrow S_{0L2}$ are responsible for weak emission at room temperature with the lifetime of about 11 and 27 μs (see Tab. 1a and Fig. S6).

Accepted Manuscript

This article is protected by copyright. All rights reserved.

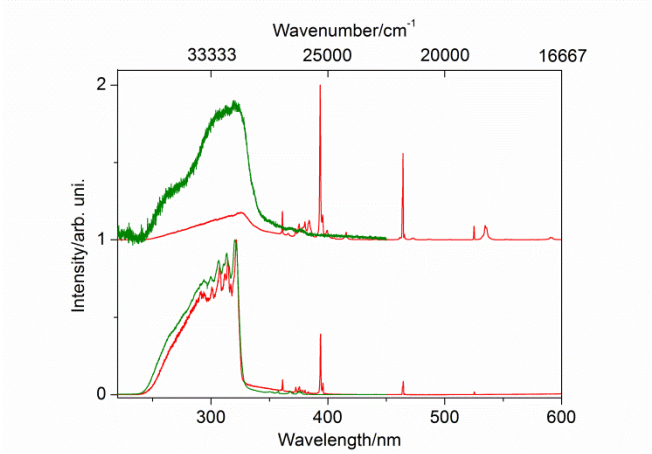

Figure 11. The excitation spectra of **2Eu** (red line, λ_{mon}=614.2 nm) and **2Tb** (green line, λ_{exc}=544.5 nm) at 293 and 77 K.

This is different from what has been observed by Souza et al. [52] for the complex with thenoyltrifluoroacetonate with the energy of barycenter of the ligand triplet state nearly the same (540 nm) as in our **2Tb** complex (555 nm). Differences in intensity of the temperature dependent sensitized emission for these both complexes may result from different mechanism of the energy transfer. Moreover, the donor-acceptor distance plays an important role. The presence of the Tb^{3+}emission in **2Tb** at 293 K additionally supports the occurrence of the $S_1 \rightarrow ff^*$ energy transfer. In the thenoyltrifluoroacetonate complex, ISC is efficient, the triplet energy transfer dominates and as such the Tb^{3+} emission ($^5D_4 \rightarrow {}^7F_5$) was observed at 60 K and lower temperatures.

In the calculations of energy transfer rates ($S_{1L1} \rightarrow ff^*$ and $T_{1L1} \rightarrow ff^*$) for **1Tb and 2Tb**, it was taken into account for the first time that the Tb^{3+} can be in its first excited electronic state ($^7F_5$), causing that new energy transfer paths become possible from S_1 to ff* levels and energy transfer from T_1 to $^5D_4$ level is facilitated also by the exchange mechanism (Tabs.S6, S8). Our motivation for this approach are the curiously long (from 2,8 to 22 ms) $^7F_5$ lifetimes, measured in glass and crystalline materials in [53,54]. This level cannot be thermally populated (lying at 2185 cm^{-1} above the ground $^7F_6$ level). The value of W_{ETS1}, when the population of $^7F_5$ is taken into account, increases from $4.39x10^6$ to $7.53x10^6$ s^{-1} for **1Tb**. The energy transfer rate from T_{1L1} to $^5D_4$ level of Tb^{3+} in **1Tb** involving $^7F_5$ (exchange mechanism) is about 100 times larger than involving the $^7F_6$ level (direct Coulomb interaction), and additionally the following new energy transfer paths become possible – from S_1 to $^5I_5$ (ΔE = 1320 cm^{-1}), $^5I_4$ (ΔE = 1698 cm^{-1}), $^5I_6$ (ΔE = 1708 cm^{-1}), $^5F_4$ (ΔE = 3932 cm^{-1}), $^5H_4$ (ΔE = 4967 cm^{-1}). These transitions are allowed through the exchange mechanism, so the **1Tb** case gives a small contribution to the intermolecular energy transfer process despite the good energy match between the S_{1L1} and the Tb^{3+} levels. This is an excellent example that sole consideration of the resonance conditions without calculation of the rate constants may lead to adverse simplification in the presentation of the energy transfer mechanisms.

For **2Tb**, the forward energy transfer rate $^5D_4 \rightarrow T_{1L2}$ ($9.4 \rightarrow 2.2x10^3$ s^{-1}) is 200 times faster than involving only the $^7F_6$ level. At the same time, values of the back energy transfer rate, $T_{1L2} \rightarrow {}^5D_4$, are about 10^7 times larger ($3.7x10^{-5} \rightarrow 2.6x10^2$ s^{-1}). Due to the very small values of the reduced matrix elements of the unit tensor operators, $\boldsymbol{U}^{(2)}$, $\boldsymbol{U}^{(4)}$ and $\boldsymbol{U}^{(6)}$, involved in the direct Coulomb interaction energy transfer rates, the forward and back energy transfer processes do not primarily involve the ground $^7F_6$ level, what is also seen in our calculations (see Tab. S8).

Theoretical calculations of the energy transfer rates, proving that the singlet energy transfer is the main pathway in the sensitization of Eu^{3+} and Tb^{3+} luminescence in the investigated complexes, correspond with the photophysical behavior of the Na and La compounds (no detectable external heavy-atom effect). The dependence of fluorescence intensity of **1Na**, **1La**, **1Eu**, **1Tb** and **2Na**, **2La**, **2Eu**, **2Tb** at 293 K is presented in Fig. 6. The intensities of fluorescence decrease in the following order: **1,2La**>>**1**,**2Tb**>**1,2Eu**. The reduction of the intensity is accompanied by a shortening of the fluorescence lifetime from 12 ns (**1La**–monoexponential fit) to 0.3 and 4.7 ns (**1Tb**-biexponential fit) for **1Ln** and from 15 ns (**2La**-monoexponential fit) to 0.03 and 7.4 ns (**2Eu**-biexponential fit) for **2Ln** (see Tab. 1).

Accepted Manuscript

This article is protected by copyright. All rights reserved.

Table 4. Experimental and calculated photophysical data for **1Eu**, **1Tb**, **2Eu**: intensity parameters $\Omega_{2,4,6}$, radiative (A_{rad}), non-radiative (A_{nrad}) decay dates, intrinsic quantum yield (Q_{Ln}^{Ln}), overall quantum yield (Q_{Ln}^{L}), sensitization efficiency (η_{sen})

	Ω_2 (10^{-20}) Ω_4 (10^{-20}) exp /cm^{-2}	Ω_2 (10^{-20}) Ω_4 (10^{-20}) Ω_6 (10^{-20}) calc /cm^{-2}	A_{rad} /s^{-1}	A_{rad}[a] /s^{-1}	A_{nrad} /s^{-1}	Q_{Ln}^{Ln}[b] /%	Q_{Ln}^{L} exp /%	Q_{Ln}^{L} calc (q) /%	η_{sens} [c] /%
1Eu	6.80 4.83	6.51· 4.74· 0.977	304	281	94	74	16.6	16.8	22
1Tb			284		76	79[d]	36		47
2Eu	8.19 2.75	7.74 2.67 1.41	307	299	255	55	10.8	11	20

Estimated error of 10% on the quantum yields Q_{Ln}^{Ln} and Q_{Ln}^{L}. [a] $1/\tau_{rad} = A_{MD,0}n^3(I_{tot}/I_{MD})$; $A_{MD,0}$=14.65 s^{-1}. [b] $Q_{Ln}^{Ln} = \frac{\tau exp}{\tau rad}$. [c] Sensitization efficiency of ligand-to-metal energy transfer $\eta_{sens} = \frac{Q_{Ln}^{L}}{Q_{Ln}^{Ln}}$. [d] Q_{Ln}^{Ln} was measured using an integrating sphere and λ_{exc} = 485.65 nm.

Comparing theoretical and experimental results for **1Eu** and **2Eu**, a very good correlation of emission quantum yields and Ω_λ parameters is obtained. The values of the overall emission quantum yields (determined and calculated), A_{rad}, A_{nrad} and Ω_λ (experimental and theoretical) are collected in Table 4. A_{rad} value was additionally calculated using the equation ($A_{rad} = A_{MD,0}n^3(I_{tot}/I_{MD})$) [55,56]. The values of Ω_2 for **1Eu** and **2Eu** are much smaller than for complexes with β-diketones [5,30] and reflect the higher local symmetry and smaller polarizability compared to β-diketonates.The emission quantum yield of **1Tb** is not very large and equals 36%. The reasons for this are the unfulfilled resonance conditions between ligand singlet state and ff* levels and also the large donor-acceptor distance. Worse matching of the S_1 state and the ff* Eu^{3+} levels is responsible for much lower emission quantum yield for **1Eu**, which is also a proof of the singlet energy transfer in the sensitization of Eu^{3+} and Tb^{3+} luminescence by sulfonylamidophosphates ligands. In the **1Ln** complexes, the total decay rates (A_{rad} + A_{nrad}) are largely dominated by the radiative contribution (A_{rad}) which corresponds to proper design of the structure of our ligands to decrease the multiphonon quenching of lanthanide emission. In the **2Eu** complex, the total decay rates are also dominated by the radiative contribution despite the low energy of ligand triplet state. It should be emphasized that the systems with the efficient energy transfer from the singlet state are very interesting because of the possibility to shift the excitation range towards lower energies.

Conclusions

The X-ray structure and spectroscopic properties of new lanthanide complexes with sulphonylamidophosphates (**1La**, **1Eu**, **1Tb**, **2La**, **2Eu**, **2Tb**) and sodium salts of the ligands (**1Na**, **2Na**) have been studied in the solid state.

This article addresses some important photophysical phenomena in lanthanide spectroscopy in the present class of new complexes.

The mechanisms of ligand-to-metal energy transfer processes occurring in this family of compounds were analyzed on the basis of experimental data and theoretical results for the first time. It was shown that the main pathway in the sensitization of Eu^{3+} and Tb^{3+} luminescence is a very rare singlet transfer. In our case this occurs mainly through the multipolar mechanism once the ligand donor state electronic barycenter is situated at a rather far distance from the lanthanide ion, practically eliminating the energy transfer process by the exchange mechanism.

Detailed, comparative studies of fluorescence intensity $S_1 \rightarrow S_0$ and its lifetime for **1Na**, **1La**, **1Eu**, **1Tb** as well as **2Na**, **2La**, **2Eu**, **2Tb** showed for the first time that ISC contribution resulting from the heavy-atom effect is not very operative in this family of complexes.

Moreover, we are the first who took into account in the theoretical calculations the higher lying excited levels of Eu (^5D_J, ^5L_J, ^5G_J) and Tb (^5D_J, ^5G_J, ^5L_J, ^5H_J, ^5F_J, ^5I_J) and we have shown their crucial role in the intramolecular energy transfer process in the present case.

Furthermore, an important role of the $^7F_5$ level of Tb^{3+} in the energy transfer process was shown. Namely new energy transfer paths became possible from S_1 to ff* levels as well as energy transfer from T_1 to $^5D_4$ level was facilitated.

The knowledge of the energy transfer mechanism allows us to choose sulphonylamidophosphates which have chromophores, that will provide good resonance conditions between the respective excited states of the donor and acceptor. This in turn will allow for planning compounds - converters of UV - Vis excitation energy with optimal luminescent properties.

Accepted Manuscript

This article is protected by copyright. All rights reserved.

The importance of the analyzed problems lies also in the possibility of their generalization and that they can be used to study the complexes of lanthanides with other groups of ligands.

Among the investigated complexes, the **1Tb** complex exhibited the highest efficiency of the energy transfer despite the long donor-acceptor distance (5.8 Å). The efficiency of the energy transfer, the very strong metal-centred emission in combination with resistance of the complexes to the UV radiation could make this family of Tb complexes promising candidates for effective UV-to-visible energy converters. This is provided that the donor-acceptor distance is shortened. This can be achieved by changing the position of the chromophore by removal solvent molecules from the intermolecular space. These investigations are currently in progress.

Experimental Section

General. Unless otherwise stated, commercially available reagent grade chemicals (Sigma-Aldrich) were used as received.

Synthesis of ligands HL^1 and HL^2

Dimethyl(4-methylphenylsulfonyl)amidophosphate – **HL^1**- was synthesized according to procedure described previously. [57, 58]

The process of obtaining dimethyl 2-naphthylsulfonyl-amidophosphate (**HL^2**) is a multistep reaction (Scheme 1.). First step was the dissolution of the naphthalene-2-sulfonyl chloride (10.60 g, 46.8 mmol) in dioxane (50 ml. AR, POCH). Resulting solution was added in portions to concentrated liquid ammonia (200 ml). After stirring for 15 minutes, the amide obtained in this reaction **(1)** was filtered off and dried in ambient air. The yield of the reaction was 91.5%. The amide (8.86 g 42.8 mmol) was refluxed with PCl_5 (8.90 g, 42.7 mmol) and CCl_4 (16 ml). The reaction was allowed to stir for 4 hours at 77°C, until a clear solution was obtained. Solvent was removed under reduced pressure. Intermediate **(2)** was obtained in 95% yield. The compound **(2)** (7.0 g, 20.4 mmol) was dissolved in dioxane (200 ml) and added dropwise to the solution of sodium methoxide in 1:4 molar ratio. Sodium methoxide was prepared by dissolving metallic sodium (1.88 g, 81.7 mmol) in methanol (100 ml). The reaction mixture was cooled down to -5°C until the combination of the substrates. The obtained solution was allowed to stir for 2 h at room temperature. The solvents were removed under reduced pressure and the resulting crude ester **(3)** was stirred and heated (80°C) with 100 ml of solution of NaOH (20%) for about 20 minutes. The resulting solution was cooled to the room temperature and filtered. The filtrate was acidified with concentrated HCl (pH=2) to give a precipitate of the title compound (**HL^2**). After the filtration, the solid was purified by recrystallization from hot isopropanol (AR, POCH). The amidophosphate (**HL^2**) was isolated in 80% yield.

^{1}H NMR (DMSO-d6, 400 MHz) δ 8.51 (s, 1H), 7.96-7.90 (m, 4H), 7.68-7.59 (m, 2H), 7.27 (s, 1H), 3.67-3.65 (d, 6H)

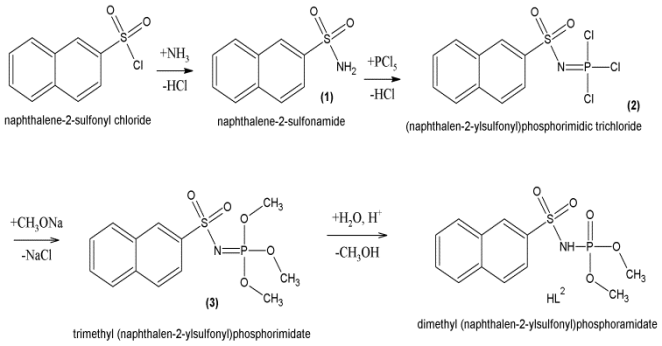

Scheme 1. Synthesis of **HL^2**.

Synthesis of sodium salt of HL^1 and HL^2.

The sodium salt of **HL^1** (**1Na**) was prepared by the reaction between equimolar amounts of sodium methylate and **HL^1**. The metallic sodium (0.09g, 4 mmol) was dissolved in methanol and added to 40 ml of a stirred solution of **HL^1** (1.20g , 4 mmol) in MeOH. The resulting solution was evaporated to obtain a white powder of **1Na**. It was purified by recrystallization from hot isopropanol.

Synthesis of sodium salt of **HL^2** (**2Na**). Sodium carbonate (0.29 g, 2.7 mmol) was dissolved in water (5ml). Subsequently, it was added in a few portions to 30 ml of a stirred solution of **HL^2** (0.85g, 2.7 mmol) in MeOH with a small amount of activated carbon. The resulting solution was allowed to stir for 0.5 h at 55°C. The mixture was filtered. The filtrate was evaporated to obtain a white powder of **2Na**.

Synthesis of the complexes.

The complexes with lanthanum, europium, and terbium with both ligands were synthesized in the same manner as the neodymium complex in the earlier article [59]. Monocrystals suitable for X-ray investigations were obtained by recrystallization from mixture of acetone and isopropanol in ratio 1:1 (complexes with **HL^1**) or by vapor diffusion from dioxane against toluene (AR, Chempur) (complexes with **HL^2**).

1Eu: yield 85%, IR(nujol) ν_{max} = 2916, 1464, 1377, 1252, 1173, 1051, 865, 745, 666, 562, 444, 333, 297, 155, 100, 73, 56 cm^{-1}; IR(fluorinated oil) ν_{max} = 3002, 2956, 2854, 2319, 1715, 1599, 1448, 1399, 1363 cm^{-1}.

2Eu: yield 67%, IR(nujol) ν_{max} = 2924, 1463, 1376, 1271, 1236 1166, 1108, 1036, 876, 838, 816, 750, 663, 645, 619, 553, 521, 479, 450, 375, 324, 280, 171 cm^{-1}; IR(fluorinated oil) ν_{max} = 2949, 2849, 1592, 1502, 1446, 1349 cm^{-1}.

Crystal structure determination. Preliminary examination and intensity data were carried out on a Kuma KM4CCD κ-axis diffractometer with graphite-monochromated MoKα radiation (λ=0.71073Å). Crystals of **2Eu** were poorly shaped and weakly diffracting, giving low resolution data. The data were corrected for Lorentz, polarization and absorption effects. The structures were solved by direct methods and refined by the full-matrix least-squares method on all F^2 data using the SHELXTL [60]. All non-hydrogen atoms were refined anisotropically. The positions of hydrogen atoms were calculated and treated as riding atoms with fixed thermal parameters. For both complexes, **1Eu** and **2Ln**, the solvent

Accepted Manuscript

This article is protected by copyright. All rights reserved.

molecules (CH_3CN and $C_4H_4O_2$) were disordered and could not be modelled properly and as such, program SQUEEZE [61] a part of the PLATON [62] package of crystallographic software, was used to calculate the solvent disorder area and remove its contribution to the overall intensity data. Moreover, the highest residual electron density peaks in **2Eu** are located near europium atoms and may be indicative of possible structural unresolved disorder. Crystallographic data for the structures reported in this paper have been deposited as supplementary publication nos. CCDC 1497264 (**1Tb**), 1497265 (**1Eu**), 1497266 (**2Eu**) and 1496876 (**2La**). These data can be obtained free of charge from The Cambridge Crystallographic Data Centre via www.ccdc.cam.ac.uk/data_request/cif.

Methods. The ^{1}H spectra in DMSO-d6 solutions were obtained on an AVANCE 400 Bruker NMR spectrometer at room temperature. Chemical shifts are reported references to $SiMe_4$ as interior standard.

The infrared spectra were recorded as nujol or fluorinated oil mull using Bruker IFS66/S FITIR spectrometer in the 50 - 4000 cm^{-1} region.

The presence of sodium salt (**1Na**, **2Na**) in the complexes (**1La**, **2La**) was excluded by determining the content of La^{3+} in examined complexes utilizing inductive coupled plasma atomic emission spectroscopy using a spectrometer (ARL Model 3410 ICP).

The high-resolution absorption spectra were recorded at room temperature with Agilent Technologies Cary 5000 Series UV-Vis-NIR Spectrophotometer.

The high-resolution emission spectra were measured with a SpectraPro 750 monochromator equipped with a Hamamatsu R928 photomultiplier and 1200 Lmm^{-1} grating blazed at 500 nm. A Xe arc lamp (450W) was used as an excitation source, coupled with a 275 cm excitation monochromator using a 1800 Lmm^{-1} grating blazed at 250 nm. These emission spectra were not corrected for the instrument response. The corrected emission spectra of Eu^{3+} complexes used for the calculations and corrected excitation spectra were recorded using an Edinburgh Instruments FLSP 920 spectrofluorometer equipped with a 150 W Xe lamp and a red-sensitive photomultiplier (Hamamatsu R-928). Fluorescence decay curves were recorded using a nF920 nanosecond flashlamp, while the phosphorescence decay curves were recorded using a µF920H 60W Xe flashlamp (Edinburgh instruments Ltd). Additionally, the phosphorescence of **1La** was excited by the 266 nm line of the Nd:YAG pulsed laser and the spectra were collected using a CCD OceanOptics SD-2000 spectrophotometer, immediately after switching off the excitation source.

The luminescence measurements were performed at room temperature and 77 K using a quartz Dewar cooled by liquid nitrogen.

Quantum yield measurements. The absolute emission quantum yield was measured at room temperature according to the method developed at the Philips Research Laboratories [63-66]. The overall emission quantum yield, Q^L_{Ln}, defined as the ratio between the number of emitted and absorbed photons, was determined according to: $U^{(\lambda)}$

$$Q^L_{Ln} = \left(\frac{1-r_{st}}{1-r_{Ln}}\right)\left(\frac{\Delta\Phi_{Ln}}{\Delta\Phi_{st}}\right) q_{st} \qquad (1)$$

where r_{st} and r_{Ln} are the amounts of exciting radiation reflected by the standard and by the sample, respectively, and q_{st} is the quantum yield of the standard phosphor. The values of r_{st}, r_{Ln}, ΔQ_{Ln} and ΔQ_{st} must be obtained for the same excitation wavelength, geometry and experimental conditions. The terms ΔQ_{Ln} and ΔQ_{st} are determined from the emission spectra, by integrating the emission intensity over the total spectral range for the sample and the standard phosphor. The Gd_2O_2S:3%Tb (GOS:Tb, q_{st} = 100%), Gd_2O_2S:3%Eu (GOS:Eu, q_{st} = 100%) and Y_2O_3:3%Eu (YOX, q_{st} = 90%) were used as the quantum yield standards. In order to have absolute values for the reflected radiation, $BaSO_4$ is used as reflectance standard (r = 91%) [5]. The errors in the quantum yield values associated with this technique were estimated to fall within 10%.

Three measurements were carried out for each sample.

Experimental Judd-Ofelt parameters. Based on the emission spectra of the **1Eu** and **2Eu** complexes, the experimental intensity parameters Ω_λ (λ = 2 and 4), radiative (A_{rad}) and non-radiative (A_{nrad}) rates, were determined from the coefficients of spontaneous emission, according to the following expression:

$$\Omega_\lambda = \frac{3\hbar c^3 A_{0\lambda}}{4e^2\omega^3\chi\left\langle {}^7F_\lambda \left\| U^{(\lambda)} \right\| {}^5D_0 \right\rangle^2} \qquad (2)$$

where χ is the Lorentz local field correction term, given by:

$$\chi = \frac{n(n^2+2)^2}{9} \qquad (3)$$

$\left\langle {}^7F_\lambda \left\| U^{(\lambda)} \right\| {}^5D_0 \right\rangle$ is a squared reduced matrix element whose value is 0.0032 for the $^5D_0 \rightarrow {}^7F_2$ transition and 0.0023 for the $^5D_0 \rightarrow {}^7F_4$ one [67]. In Eq.(2) *e* is the electron charge, *ħ* is Planck's constant, *n* is the reflective index, *c* – speed of light and *ω* that is the frequency of the transition. The $A_{0\lambda}$ (λ = 2 and 4), are spontaneous emission coefficients, calculated by taking the magnetic dipole transition $^5D_0 \rightarrow {}^7F_1$ as the reference, as this transition is practically insensitive to the chemical environment around the europium ion. The following expression was used [5]:

$$A_{0\lambda} = A_{01}\left(\frac{S_{0\lambda}}{S_{01}}\right)\left(\frac{\sigma_{01}}{\sigma_{0\lambda}}\right) \quad (4)$$

where S_{01} and $S_{0\lambda}$ are the areas under the curves of the $^5D_0 \rightarrow {}^7F_1$ and $^5D_0 \rightarrow {}^7F_\lambda$ transitions, with σ_{01} and $\sigma_{0\lambda}$ being their energy barycenters, respectively. The coefficient of spontaneous emission, A_{01}, in equation (4) is given by the relation $A_{01} = 0.31 \cdot 10^{-11}((n^3)(\sigma_{01})^3$. Refractive indexes were determined by the immersion method.

Theoretical calculations. The energy transfer between the ligand and the Ln^{3+} ion involves the singlet-triplet (spin - forbidden) and the singlet-singlet (spin - allowed) bands of the ligand and the $\alpha' J' \leftrightarrow \alpha J$ transition lines of the Ln^{3+}ion. This process was treated in terms of the direct Coulomb and the exchange interactions [27,28]. For the Coulomb interaction the transfer rate is given by:

$$W_{Cl} = \sum_{\lambda=2,4,6} \frac{e^2 S_L}{G(2J+1)}\left(\frac{\Omega^{ed}_\lambda}{R^6_L} + \frac{(\lambda+1)\langle r^\lambda\rangle^2\langle 3\|C^{(\lambda)}\|3\rangle^2(1-\sigma_\lambda)^2}{S_L\left(R^{\lambda+2}_L\right)^2}\right)\left|\langle \alpha' J' \| U^{(\lambda)} \| \alpha J\rangle\right|^2 \quad (5)$$

where *J* and *J'* represent the total angular momentum of the Ln^{3+} ion electronic states involved in energy transfer process. S_L is the dipole strength of the ligand transition, *G* stands for the degeneracy of the donor state and Ω^{ed}_λ are the contributions of the forced electric dipole mechanism to the 4f – 4f transition intensity parameters (Judd – Ofelt theory). $\langle r^\lambda\rangle$ are the 4f radial integrals, σ_λ are the shielding factors due to shielding effects produced by the filled 5s and 5p sub-shells, R_L is the distance from the Ln^{3+} ion nucleus to the barycenter of the ligand electronic state and $U^{(\lambda)}$ are unit tensor operators. The exchange intramolecular energy transfer rate (W_{Ex}) is given by [27]:

Accepted Manuscript

This article is protected by copyright. All rights reserved.

$$W_{Ex}=\frac{\langle 4f|L\rangle^4}{(2J+1)}\frac{8\pi e^2}{3\hbar R_L^4}\left|\langle \alpha' J'\|S\|\alpha J\rangle\right|^2\left|\langle\varphi|\sum_i \mu_z(i)s_m(i)|\varphi^*\rangle\right|^2 F \qquad (6)$$

$\langle 4f|L\rangle$ is the overlap integral between the 4f orbitals and ligand eigenfunctions, S_m is a spherical component of the spin operator of electron *i* in the ligand, μ_z is the z-component of its dipole operator, *F* is the donor-acceptor spectral overlap that depends on the appropriate energy mismatch conditions and *S* is the total spin operator of the Ln^{3+} ion. The selections rules on *J* are obtained using the reduced matrix elements of the unit tensor operators $U^{(\lambda)}$ and those for the total spin operator *S*. From the above matrix elements, as far as *J* is considered a good quantum number, the selection rules are $|J\text{-}J'|=0$ or 1, for the exchange mechanism, and $J'\text{-}J \le \lambda \le J+J'$ for the Coulomb mechanism, in both cases J'=J=0 excluded.

The spectral overlap factor has been given by the following expression [28]

$$F = \frac{1}{\hbar\gamma}\sqrt{\frac{\ln(2)}{\pi}}\,exp\left[-\left(\frac{\Delta}{\hbar\gamma}\right)^2\ln(2)\right] \qquad (7)$$

where ħγ is the (barycenter) band width at half-height of the appropriate transition in the ligand and Δ is the difference between this transition energy and the energy barycenter of the α'J'↔αJ transition. For back transfer, the rates should be multiplied by the activation energy barrier Boltzmann factor $e^{\frac{-\Delta}{kT}}$ [51]

Calculated quantum yield. The appropriate rate equations were solved analytically corresponding to the energy level diagram in Figs. 9,10, by assuming that under low power excitation, the normalized population of the ground state is equal to one. The theoretical result for the luminescence quantum yield is given by:

$$q=\left(\frac{\sigma_{Em}}{\sigma_{Abs}}\right)A_{rad}\tau\left[\frac{1}{\tau_S^{-1}+W_{ETS}}\right]\left[W_{ETS}+\frac{W_{ETT}}{\left[\left(\tau_T^{-1}+W_{ETT}\right)\tau_S\right]}\right] \qquad (8)$$

where τ is the lifetime of the $^5D_0$ (Eu^{3+}) or $^5D_4$ (Tb^{3+}) levels, τ_S and τ_T are the decay times respectively of the singlet and triplet states, $\frac{\sigma_{Em}}{\sigma_{Abs}}$ is the ratio between the energy barycenters of the transitions.

All calculations were made by using program Mathcad 14.0@.

Acknowledgements

The authors wish to acknowledge support through the grant of Minister of Science and Higher Education POIG.01.01.02-02-006/09 and the grant Minister of Science and Higher Education for young scientists 2432/M/WCH/14.

Keywords: lanthanide • luminescence • sulphonylamidophosphates • energy transfer • crystal structure

[1] *Lanthanide Luminescence Photophysical, Analytical and Biological Aspects, Vol. 7* (Eds: P. Hänninen, H. Härma), Springer-Verlag, Berlin Heidelberg, **2011**.

[2] N. Sabbatini, M. Guardigli, J.-M. Lehn, *Coord. Chem. Rev.* **1993**, *123*, 201-228.

[3] E. Huskowska, P. Gawryszewska, J. Legendziewicz, C. L. Maupin, J. P. Riehl, *J. All. Comp.* **2000**, *303-304*, 325-330.

[4] Y. Gerasymchuk, L. Tomachynski, M. Guzik, A. Koll, J. Jański, Y. Guyot, W. Stręk, G. Boulon J. Legendziewicz, *J. Photochem. Photobio. A* **2015**, *309*, 65–71.

[5] G. F. de Sá, O. L. Malta, C. de Mello Donegá, A. M. Simas, R. L. Longo, P. A. Santa-Cruz, E. F. da Silva Jr., *Coord.Chem.Rev.* **2000**, *196*, 165-195.

[6] P. Gawryszewska, O. L. Malta, R. L. Longo, F. R. Gonçalves e Silva, S. Alves, K. Mierzwicki, Z. Latajka, M. Pietraszkiewicz, J. Legendziewicz, *ChemPhysChem* **2004**, *5*, 1577-1584.

[7] J.-C. G. Bünzli, *Coord. Chem. Rev.* **2015**, *293-294*, 19–47.

[8] M. J. Kleinerman, *J. Chem. Phys.* **1969**, *51*, 2370–2375.

[9] E. Huskowska, I. Turowska-Tyrk, J. Legendziewicz, J. P. Riehl, *New J. Chem.* **2002**, *26*, 1461-1467.

[10] G. A. Hebbink, A. I. Klink, L. Grave, P. G. B. Oude Alink, F. C. J. M. van Veggel, *ChemPhysChem* **2002**, *3*, 1014-1018.

[11] M. H. V. Werts, J. W. Hofstraat, F. A. J. Geurts, J. W. Verhoeven, Chem. *Phys. Lett*. **1997**, *276*, 196-201.

[12] F. Vögtle, M. Gorka, V. Vicinelli, P. Ceroni, M. Maestri, V. A. Balzani, *ChemPhysChem* **2001**, *12*, 769-773.

[13] V. Vicinelli, P. Ceroni, M. Maestri, V. Balzani, M. Gorka, F. Vögtle, *J. Am. Chem. Soc.* **2002**, *124*, 6461-6468.

[14] F. R. Gonçalves e Silva, O. L. Malta, C. Reinhard, H.-U. Güdel, C. Piguet, J. E. Moser, J.-C. G. Bünzli, *J. Phys. Chem. A* **2002**, *106*, 1670-1677.

[15] J. R. G. Thorne, J. M. Rey, R. G. Denning, S. E. Watkins, M. Etchells, M. Green, V. Christou, *J. Phys. Chem. A* **2002**, *106*, 4014-4021.

[16] I. Mekkaoui Alaoui, *J. Phys. Chem.* **1995**, *99*, 13280-13282.

[17] J. Andres, A.-S. Chauvin, *Phys. Chem. Chem. Phys.* **2013**, *15*, 15981-15994.

[18] V. F. Plyusnin, A. S. Kupryakov, V. P. Grivin, A. H. Shelton, I. V. Sazanovich, A. J. H. M. Meijer, J. A. Weinstein, M. D. Ward, *Photochem. Photobiol. Sci*. **2013**, *12*, 1666-1679.

[19] J. Bruno, W. D. Horrocks Jr., R. J. Zauhar, *Biochemistry* **1992**, *31*, 7016–7026.

[20] A. Guenet, F. Eckes, V. Bulach, C. A. Strassert, L. De Cola, M. W. Hosseini, *ChemPhysChem* **2012**, *13*, 3163-3171.

[21] J. H. Ryu, Y. K. Eom, J.-C. G. Bünzli, H. K. Kim, *New J. Chem.* **2012**, *36*, 723–731.

[22] V. V. Utochnikova, A. D. Kovalenko, A. S. Burlov, L. Marciniak, I. V. Ananyev, A. S. Kalyakina, N. A. Kurchavov, N. P. Kuzmina, *Dalton Trans.* **2015**, 44, 12660-12669.

[23] P. Guerriero, P. A. Vigato, J.-C. G. Bünzli, E. Moret, *J. Chem. Soc., Dalton Trans.* **1990**, *2*, 647–655.

[24] R. C. Howell, K. V. N. Spence, I. A. Kahwa, A. J. P. White, D. J. Williams, *J. Chem. Soc., Dalton Trans*. **1996**, *6*, 961–968.

[25] R. Rodríguez-Cortiñas, F. Avecilla, C. Platas-Iglesias, D. Imbert, J.-C. G. Bünzli, A. Blas, T. Rodríguez-Blas, *Inorg. Chem.* **2002**, *41*, 5336–5349.

[26] M. A. Katkova, A. V. Borisov, G. K. Fukin, E. V. Baranov, A. S. Averyushkin, A. G. Vitukhnovsky, M. N. Bochkarev, *Inorg. Chim. Acta* **2006**, *359*, 4289–4296.

[27] O. L. Malta, *J. Non-Cryst. Solids* **2008**, *354,* 4770-4776.

[28] O. L. Malta, J. Legendziewicz, E. Huskowska, I. Turowska-Tyrk; R. Q. Albuquerque, C. De Mello Donegá, F. R. Gonçalves e Silva, *J. Alloys Compd.* **2001**, *323-324*, 654-660.

[29] O. L. Malta, *J. Lumin.* **1997**, *71*, 229-236.

[30] K. Binnemans in *Handbook on the Physics and Chemistry of Rare Earths, Vol. 35* (Eds.: K. A. Gschneidner Jr., J.-C. G. Bünzli, V. K. Pecharsky) Elsevier Science B.V, Amsterdam, **2005**, pp 107-272.

[31] J. Kai, M. C. F. C. Felinto, L. A. O. Nunes, O. L. Malta, H. F. Brito, *J. Mater. Chem.* **2011**, *21*, 3796-3802.

[32] P. P. Lima, M. M. Nolasco, F. A A. Paz, R. A. S. Ferreira, R. L. Longo, O. L. Malta, L. D. Carlos, *Chem. Mater.* **2013**, *25*, 586-598.

[33] E. B. Gibelli, J. Kai, E. E. S. Teotonio, O. L. Malta, M. C. F. C. Felinto, H. F. Brito, *J. Photochem. Photobiol., A* **2013**, *251*, 154-159.

Accepted Manuscript

This article is protected by copyright. All rights reserved.

[34] D. Kulesza, M. Sobczyk, J. Legendziewicz, O. M. Moroz, V. Amirkhanov, *Struct. Chem.* **2010**, *21*, 425-438.
[35] P. Gawryszewska, O. V. Moroz, V. A. Trush, D. Kulesza, V. M. Amirkhanov, *J. Photochem. Photobiol., A* **2011**, *217*, 1-9.
[36] P. Gawryszewska. O. V. Moroz, V. Trush, V. M. Amirkhanov, T. Lis, M. Sobczyk, M. Siczek, *ChemPlusChem* **2012**, *77*, 482-496.
[37] P. Gawryszewska, V. M. Amirkhanov, V. A. Trush, D. Kulesza, J. Legendziewicz, *J. Lumin.* **2016**, *170*, 340–347.
[38] M. Sobczyk, K. Korzeniowski, M. Guzik, V. M. Amirkhanov, V. A. Trush, P. Gawryszewska, Y. Guyot, G. Boulon, W. Stręk, J. Legendziewicz, *J. Lumin*. **2016**, *169*, 777-781.
[39] M. A. Porai-Koshits, L. A. Aslanov, *Zh. Strukt. Khim*. **1972**, *13*, 244-253.
[40] I. O. Shatrava, T. Y. Sliva, V. A. Ovchynnikov, I. S. Konovalova, V. M. Amirkhanov, *Acta Cryst*. **2010**, *E66*, m397-m398.
[41] O. V. Moroz, V. A. Trush, I. S. Konovalova, O. V. Shishkin, Y. S. Moroz, S. Demeshko, V. M. Amirkhanov, *Polyhedron* **2009**, *28*, 1331-1335.
[42] Y. Umezawa, S. Tsuboyama, K. Honda, J. Uzawa, M. Nishio, *Bull. Chem. Soc. Jpn.* **1998**, *71*, 1207-1213**.**
[43] W.M. Faustino, O. L. Malta, G. F.de Sá, *J. Chem. Phys.* **2005**, *122*, 054109-054119.
[44] F. J. Steemers, W. Verboom, D. N. Reinhoudt, E. B. van der Tol, J. W. Verhoeven, *J. Am. Chem. Soc*. **1995**, *117*, 9408-9414.
[45] P. A. Tanner, *Chem. Soc. Rev.* **2013**, *42*, 5090-5101.
[46] J. H. Försberg, *Coord. Chem. Rev.* **1973**, *10*, 195 -226.
[47] G. Blasse, G. J. Dirksen, J. P. M. Vanvliet, *Inorg. Chim. Acta* **1988**, *142*, 165-168.
[48] P. Gawryszewska, L. Z. Ciunik, *J. Photochem. Photobiol., A*, **2009**, *202*, 1-9.
[49] E. Kasprzycka, V. A. Trush, V. M. Amirkhanov, L. B. Jerzykiewicz, P. Gawryszewska, *Opt. Mater. (Amsterdam, Neth.)* **2014**, *37*, 476-482.
[50] N. Pawlak, G. Oczko, *Polyhedron* **2014** *74,* 31-38.
[51] W. M. Faustino, L. A. Nunes, I. A. A. Terra, M. C. F. C. Felinto, H. F. Brito, O. L. Malta, *J. Lumin.* **2013**, *137*, 269-273.
[52] A. S. Souza, L. A. Nunes, M. C. F. C. Felinto, H. F. Brito, O. L. Malta, *J. Lumin.* **2015**, *167*, 167-171.
[53] U. N. Roy, R. H. Hawrami, Y. Cui, S. Morgan, A. Burger, K. C. Mandal, C. C. Noblitt, *Appl. Phys. Lett.* **2005**, *86*, 151911-1-151911-3.
[54] K. Rademaker, W. F. Krupke, R. H. Page, S. A. Payne, K. Peterman, G. Huber, A. P. Yelisseyev, L. I. Isaenko, U. N. Roy, A. Burger, K. C. Mandal, K. Nitsch, *J. Opt. Soc. Am. B* **2004**, *21*, 2117-2129.
[55] E. B. van der Tol, H. J. van Ramesdonk, J. W. Verhoeven, F. J. Steemers, E. G. Kerver, W. Verboom, D. N. Reinhoudt, *Chem. Eur. J.* **1998**, *4,* 2315-2323.
[56] M. H. V. Werts, R. T. F. Jukes, J. W. Verhoeven, *Phys. Chem. Chem. Phys.* **2002**, *4*, 1542-1548.
[57] A. V. Kirsanov, *Zh. Obsh. Khim* **1954**, *24*, 474-484.
[58] V. M. Amirkhanov, V. Ovchynnikov, V. A. Trush, P. Gawryszewska, L. B. Jerzykiewicz in *Ligands: Synthesis, Characterization and Role in Biotechnology* (Eds.: P. Gawryszewska, P. Smoleński) NOVA, New York, **2014**, pp 199-248.
[59] E. Kasprzycka, V. A. Trush, L. B. Jerzykiewicz, V. M. Amirkhanov, P. Gawryszewska, *J. Lumin*, **2016**, *170*, 348-356.
[60] G. M. Sheldrick, SHELXTL Version 2014/7. http://shelx.uni-ac.gwdg.de/SHELX/index.php.
[61] P. van der Sluis, A. L. Spek, *Acta Cryst.* **1990**, *A46*, 194–201.
[62] A. L. Spek, *Acta Cryst.* **1990**, *A46*, C34– C36.
[63] A. Bril in *Luminescence of Organic and Inorganic Materials* (Eds.:H. P. Kallman, G. M. Spruch) Wiley, Eindhoven, **1962**, pp. 479-493.
[64] A. Bril, A. W. De Jager-Veenis, *J. Res. Natl. Bureau Stand* **1976,** *80 A*, 401-408.
[65] A. Bril, A. W. De Jager-Veenis, *J. Electrochem. Soc.* **1976**, *123,* 396-398.
[66] A. W. De Jager-Veenis, A. Bril, *Philips J. Res.* **1978,** *33*, 124-132.
[67] W. T. Carnall, P. R. Fields, K. Rajnak, *Chemistry Division Report* **1967**.

Accepted Manuscript

This article is protected by copyright. All rights reserved.

10.1002/chem.201603767

WILEY-VCH

Entry for the Table of Contents (Please choose one layout)

Layout 1:

FULL PAPER

Text for Table of Contents

((Insert TOC Graphic here: max. width: 5.5 cm; max. height: 5.0 cm))

*Author(s), Corresponding Author(s)**

Page No. – Page No.

Title

Layout 2:

FULL PAPER

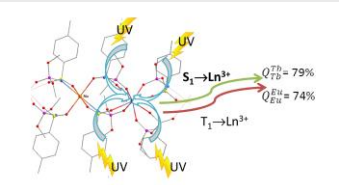

The rarely observed singlet state energy transfer was proved to be a dominant mechanism in the new class of lanthanide complexes. This is strongly evidenced by theoretical calculations using the higher lying excited levels of Eu (^5D_J, ^5L_J, ^5G_J) and Tb (^5D_J, ^5G_J, ^5L_J, ^5H_J, ^5F_J, ^5I_J) for the first time. Photophysical properties make this family of Tb complexes promising candidates for effective UV-to-visible energy converters.

*Author(s), Corresponding Author(s)**

Page No. – Page No.

Title

Accepted Manuscript

This article is protected by copyright. All rights reserved.